Geol. Mag. **149** (*5*), *2012, pp. 753–767. © Cambridge University Press 2011*
doi:10.1017/S0016756811000987

Genesis of the Chehugou Mo-bearing granitic complex on the northern margin of the North China Craton: geochemistry, zircon U–Pb age and Sr–Nd–Pb isotopes

QING-DONG ZENG*, JIN-HUI YANG, JIAN-MING LIU, SHAO-XIONG CHU, XIAO-XIA DUAN, ZUO-LUN ZHANG, WEI-QING ZHANG & SONG ZHANG

Key Laboratory of Mineral Resources, Institute of Geology and Geophysics, Chinese Academy of Sciences, P. O. Box 9825, Beijing 100029, China

(*Received* 21 March 2011; *accepted* 7 October 2011; *first published online* 24 November 2011)

Abstract – The Chehugou granite-hosted molybdenum deposit is typical of the Xilamulun metallogenic belt, which is an important Mo–Ag–Pb–Zn producer in China. A combination of major and trace element, Sr and Nd isotope, and zircon U–Pb isotopic data are reported for the Chehugou batholith to constrain its petrogenesis and Mo mineralization. The zircon SIMS U–Pb dating yields mean ages of 384.7 ± 4.0 Ma and 373.1 ± 5.9 Ma for monzogranite and syenogranite and 265.6 ± 3.5 Ma and 245.1 ± 4.4 Ma for syenogranite porphyry and granite porphyry, respectively. The Devonian granites are calc-alkaline with K_2O/Na_2O ratios of 0.44–0.52, the Permian granites are alkali-calcic with K_2O/Na_2O ratios of 1.13–1.25, and the Triassic granites are calc-alkaline and alkali-calcic rocks with K_2O/Na_2O ratios of 0.78–1.63. They are all enriched in large-ion lithophile elements (LILEs) and depleted in high-field-strength elements (HFSEs) with negative Nb and Ta anomalies in primitive mantle-normalized trace element diagrams. They have relatively high Sr (189–1256 ppm) and low Y (3.87–5.43 ppm) concentrations. The Devonian granites have relatively high initial Sr isotope ratios of 0.7100–0.7126, negative $\varepsilon_{Nd}(t)$ values of −12.3 to −12.4 and $^{206}Pb/^{204}Pb$ ratios of 16.46–17.50. In contrast, the Permian and Triassic granitoids have relatively low initial $^{87}Sr/^{86}Sr$ ratios (0.7048–0.7074), negative $\varepsilon_{Nd}(t)$ values of −10.1 to −13.1 and $^{206}Pb/^{204}Pb$ ratios of 17.23–17.51. These geochemical features suggest that the Devonian, Permian and Triassic Chehugou granitoids were derived from ancient, garnet-bearing crustal rocks related to subduction of the Palaeo-Asian Ocean and subsequent continent–continent collision between the North China and Siberian plates.

Keywords: Chehugou granitic complex, partial melting, U–Pb zircon age, northern margin of North China Craton.

1. Introduction

The Xilamulun metallogenic belt on the northern margin of the North China Craton (NCC) is an important Mo–Ag–Pb–Zn producer in China (Fig. 1). The Xilamulun metallogenic belt extends E–W for approximately 400 km and S–N for 100 km. It contains medium- to large-scale molybdenum deposits, such as the Chehugou, Xiaodonggou, Jiguanshan, Nianzigou, Baimashi and Kulitu deposits, and their discovery was an important breakthrough in recent years for mineral exploration on the northern margin of the NCC (Zeng *et al*. 2011*a*). Previous studies suggested that the mineralization occurred during the Yanshanian period (Rui, Shi & Fang, 1994). However, recent studies show that the Indosinian period is also an important ore-forming epoch in the Xilamulun metallogenic belt (Zeng *et al*. 2011*a*; Liu *et al*. 2010). The ore-forming epoch in the Xilamulun metallogenic belt includes three stages: Early Triassic, Late Jurassic and Early Cretaceous. The Chehugou and Kulitu deposits are the only Triassic deposits. The Late Jurassic Mo deposits and granitoids are related to Palaeo-Pacific tectonic evolution, and the Early Cretaceous Mo deposits and granitoids are related to lithosphere thinning in east China (Zeng *et al*. 2011*a*). All studies on the Xilamulun metallogenic belt show that the Mo mineralization is related to the granitoids in genesis (Nie *et al*. 2007; Qin *et al*. 2009; Wan *et al*. 2009; Zeng *et al*. 2009, 2010, 2011*a*; Chen *et al*. 2010; Liu *et al*. 2010; Zhang *et al*. 2009; Wu *et al*. 2008, 2011).

The Chehugou Mo deposit is granite hosted. Wan *et al*. (2009) reported a Rb–Sr isochron age of *c*. 256 Ma for chalcopyrite from the Chehugou Mo deposit that suggested its mineralization age was Late Permian. They proposed that the metallogenesis had a genetic relationship with the syenogranites. Recently, Zeng *et al*. (2011*a*) obtained a Re–Os isochron age for molybdenite from the Chehugou Mo deposit that showed that the Chehugou Mo deposit was formed in the Triassic period and that the metallogenesis had a relationship with the Triassic granite porphyry in the deposit area. Furthermore, Liu *et al*. (2010) proposed that the Mo deposit was formed during the Late Permian period according to the Re–Os isochron age (257 Ma) of molybdenite from the NE-trending Cu–Mo veins

*Author for correspondence: zengqingdong@mail.iggcas.ac.cn

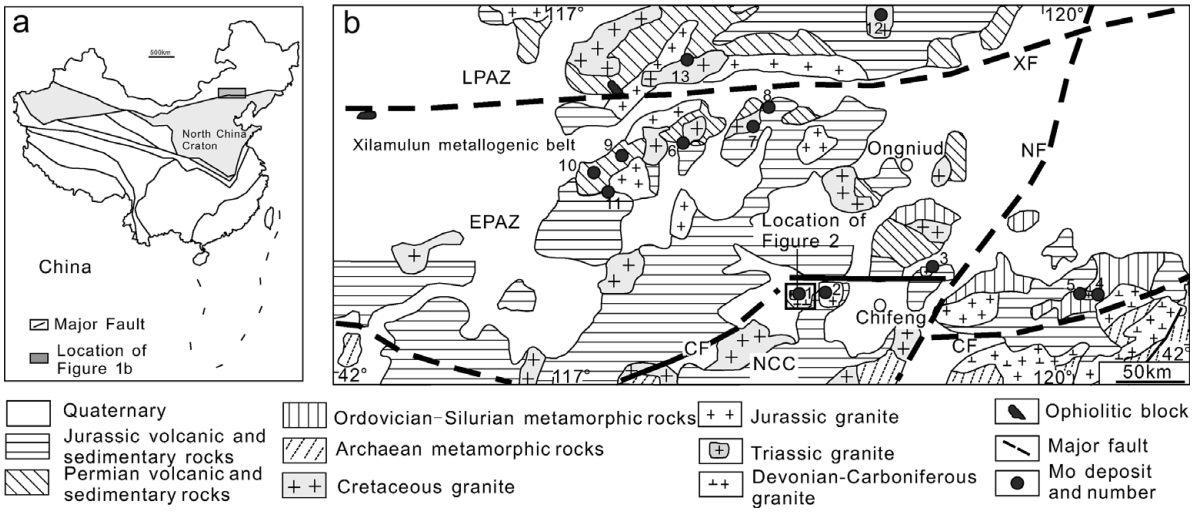

Figure 1. Regional geological map of the Chehugou (adapted from Zeng *et al*. 2011*b*). NCC – North China Craton; EPAZ – Early Palaeozoic accretion zone; LPAZ – Late Palaeozoic accretion zone; XF – Xilamulun River Fault; NF – Neijiang Fault; CF – Chifeng Fault. Molybdenum deposit names: 1 – Chehugou; 2 – Nianzigou; 3 – Jiguanshan; 4 – Kulitu; 5 – Baimashi; 6 – Xiaodonggou; 7 – Gangzi; 8 – Tuohe; 9 – Hongshanzi; 10 – Xinfangzi; 11 – Talagou; 12 – Yangchang; 13 – Longtoushan.

of the Chehugou deposit and that the metallogenesis was structurally controlled. However, Rui, Shi & Fang (1994) suggested that the granitoid in this area formed during the Late Indosinian–Yanshanian period (205–135 Ma). To understand the metallogenesis of the Mo deposit and its genetic relationship to the host granites, we present the whole-rock elemental geochemistry, Sr–Nd–Pb isotope geochemistry and U–Pb zircon geochronology of the host granitoids for the Chehugou deposit, to constrain the ages and petrogenesis of the host granitoids and assess the broader tectonomagmatic implications of the Chehugou Mo deposit and its host granites. Our results have significant implications for constraining the molybdenum resource of the Mo deposit.

2. Geological setting and petrography

The Chehugou area is divided into two parts by the Chifeng Fault on the northern margin of the NCC (Fig. 1). The NCC lies to the south of the fault and the Early Palaeozoic accretion zone (EPAZ) in the north. The crystalline basement of the NCC is composed of Archaean gneiss and granite, whereas the EPAZ is mainly composed of Ordovician–Silurian metamorphic rocks and Permian and Jurassic volcanic and sedimentary rocks. There is a Late Palaeozoic accretion zone to the north of the Xilamulun River Fault, which is mainly composed of Permian volcanic and sedimentary rocks. The intrusive rocks in the area mainly include Jurassic and Cretaceous granitic intrusions (BGMR, 1991; Zeng *et al*. 2010, 2011*a*).

The Chehugou Mo deposit is located in the Chehugou granitic complex, which consists of monzogranite, syenogranite, syenogranite porphyry and granite porphyry, with an outcrop area of 30 km^2. Mafic enclaves commonly occur throughout the monzogranite and syenogranite. The syenogranite porphyry intrudes into the syenogranite and monzogranite. The granite porphyry occurs as a stock and intrudes into the monzogranite and syenogranite (Fig. 2).

The monzogranite is typically porphyritic, with megacrysts of K-feldspar (up to 5 cm in length) and subordinate plagioclase (up to 3 cm in length), which commonly represent ~ 15 % of the rock. K-feldspar is generally perthitic (Fig. 3a). Plagioclase is generally automorphic and subhedral, and is twinned. The matrix mineral assemblage includes perthite (40 %), plagioclase (30 %), quartz (25 %) and biotite (5 %), with or without minor hornblende. Accessory minerals include apatite, zircon, titanite and magnetite.

The syenogranite is fine grained (Fig. 3b) and consists of 50–55 % alkali feldspar, 20–30 % plagioclase, 20–30 % quartz and minor (<1 %) biotite. Accessory minerals include magnetite, zircon and apatite.

The syenogranite porphyry is typically porphyritic, with crystals of orthoclase, which commonly represent ~ 5–15 % of the rock (Fig. 3c). The matrix mineral assemblage includes quartz, orthoclase, plagioclase and biotite. Accessory minerals include magnetite, zircon and apatite.

The granite porphyry is typically porphyritic, with crystals of quartz, plagioclase and K-feldspar, which commonly represent 20 % of the rock (Fig. 3d). The matrix mineral assemblage includes quartz, K-feldspar and plagioclase, with minor biotite. Accessory minerals include magnetite, zircon and apatite. Silicification and kaolinization are developed in the granite porphyry stock.

The major intrusive rocks in the ore area were sampled and analysed to determine the timing of the magma intrusive activities, the sources of metals and to infer the ore-forming tectonic environment.

https://doi.org/10.1017/S0016756811000987 Published online by Cambridge University Press

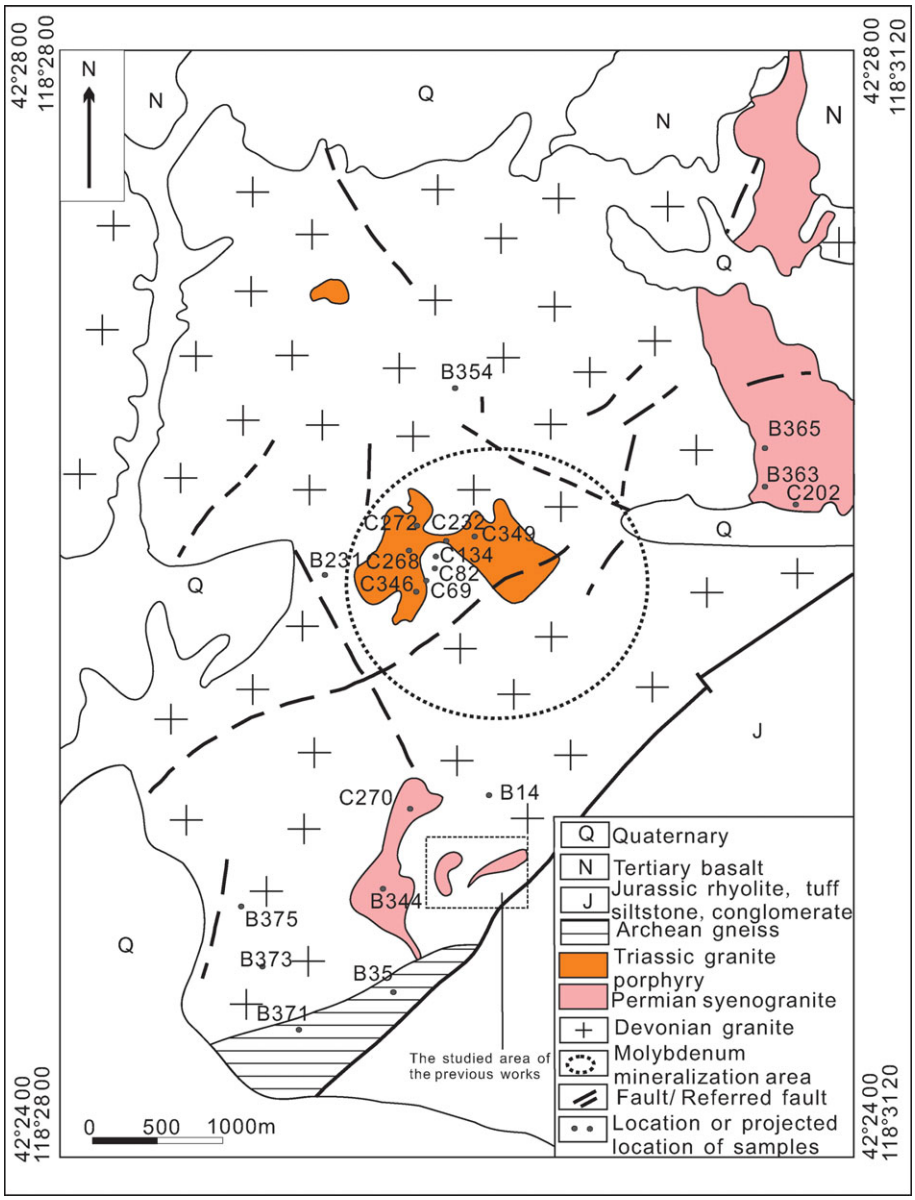

Figure 2. (Colour online) Simplified geological map of the Chehugou Mo deposit (modified from No. 243 Team, unpub. survey report of the Chehugou Mo deposit, 2007).

3. Analytical methods

Samples were crushed into granules less than 200 mesh and then analysed for major and trace elements and isotopes. The samples were analysed at the State Key Laboratory of Lithospheric Evolution, Institute of Geology and Geophysics, Chinese Academy of Sciences. Major elements were determined by X-ray fluorescence (XRF), with analytical uncertainties ranging from 1 to 3 %. Trace element (including rare earth element; REE) concentrations were determined by inductively coupled plasma mass spectrometry (ICP-MS) with an ELEMENT system. According to Chinese national standards GSR-1 and GSR-2, the error was <5 % for trace elements with concentrations >10 ppm and <10 % for trace elements with contents <10 ppm (Gao *et al*. 2002).

Rb, Sr, Sm and Nd isotopes were analysed using a MAT-262 thermal ionization mass spectrometer (TIMS). The detailed analytical procedures are described by Chen, Hegner & Todt (2000) and Chen *et al*. (2002). About 100 mg of a whole-rock powder sample were weighed, and then appropriate amounts of ^{87}Rb–^{84}Rb and ^{149}Sm–^{150}Nd mixed diluent and purified HF–$HClO_4$ mixed acid were added so as to fully dissolve the sample at a high temperature. Separation and purification were carried out in a quartz exchange column filled with 5 ml of AG 50W-X12 exchange resin (200–400 mesh) for Rb and Sr, and in a quartz exchange column with 1.7 ml of Teflon powder as the exchange medium for Sm and Nd. Isotope ratios of $^{146}Nd/^{144}Nd = 0.7219$ and $^{86}Sr/^{85}Sr = 0.1194$ were adopted for correction of obtained Nd and Sr isotope ratios, respectively. The results of standard samples BCR and NBS987 were $^{143}Nd/^{144}Nd = 0.512630 \pm 7$ ($n = 45$) and $^{87}Sr/^{86}Sr = 0.710221 \pm 4$ ($n = 100$), respectively. The blanks were about 100 pg for Rb and Sr and

https://doi.org/10.1017/S0016756811000987 Published online by Cambridge University Press

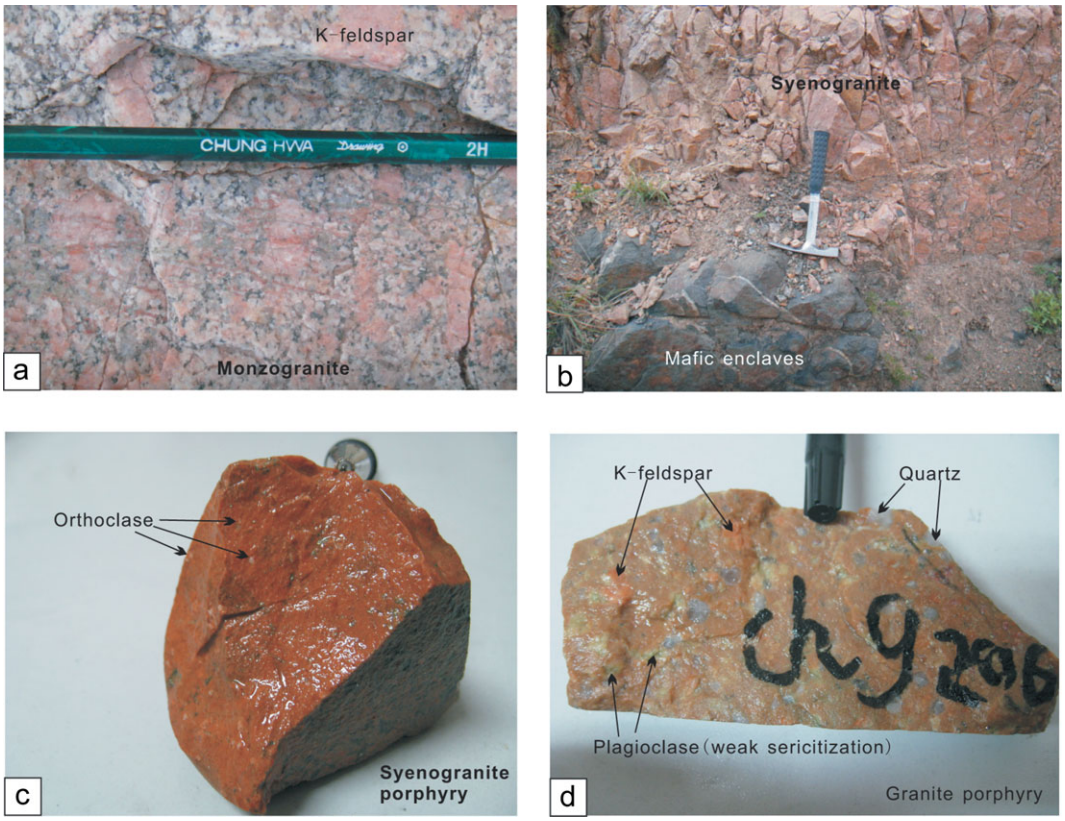

Figure 3. (Colour online) Photographs of major intrusive rocks in the Chehugou area. (a) Monzogranite; (b) syenogranite (containing mafic enclave); (c) syenogranite porphyry; (d) granite porphyry.

about 50 pg for Sm and Nd, respectively. The errors on $^{147}Sm/^{144}Nd$ and $^{87}Rb/^{86}Sr$ were less than 0.5 %.

The Pb isotopes were analysed using a MAT-262 TIMS. HF acid was used to dissolve the sample, and the sample solution was dried by evaporation. A 6N HCl solution was employed to convert the fluorinated sample into chloride, which was dried by evaporation, and then 0.6N HBr was used for sample extraction. Flows of 0.6N HBr and 6N HCl were adopted to separate and purify the Pb sample in a Teflon exchange column filled with 80 μl of AGl-X8 (100–200 mesh) exchange resin. The result for the Pb standard sample NBS981 was $^{207}Pb/^{206}Pb = 0.9138$ ($n = 37$), and the whole-flow background for Pb was less than 50 pg (Chen, Hegner & Todt, 2000; Chen *et al*. 2002).

The U–Th–Pb isotopic analysis of zircon for the granite porphyry and syenogranite porphyry was carried out with a sensitive high-resolution ion microprobe (SHRIMP) II instrument at the Beijing SHRIMP Centre. Standard zircon TEMORA 1 (417 Ma, Black *et al*. 2003) was used to correct $^{206}Pb/^{238}U$, and SL13 (with a U content of 238 ppm and average Th/U = 0.09, Black *et al*. 2003) was used to standardize the U and Th contents in samples; data processing was conducted using SQUID1.0 and Isoplot 3.2 (Ludwig, 2001). For the detailed test principles and analysis and data-processing flows, see Song, Zhang & Wan (2002). The measured ^{204}Pb was used to correct the common Pb content in zircon, and the single-point analysis errors were at the 1σ level; the result was the average $^{206}Pb–^{238}U$ age with a confidence of 95 %.

The U–Th–Pb isotope analysis of zircon for the monzonitic granite and syenogranite was conducted with a Cameca IMS-1280 ion microprobe at the Institute of Geology and Geophysics, Chinese Academy of Sciences. U–Th–Pb isotope ratios were obtained through correction with standard zircon Plesovice (Sláma *et al*. 2008). The U and Th contents were obtained through correction with standard zircon 91500 (Li *et al*. 2009). For the detailed test flow and data-processing method, see Li *et al*. (2009) and Stacey & Kramers (1975). The measured ^{204}Pb value was used for correction of common Pb content. Because the common Pb content was very low, it could be thought that the common Pb was mainly from surface Pb contamination during sample preparation, and the average Pb isotope composition in the modern crust was used as the common Pb composition for correction. The single-point analysis error for the isotope ratio and age was reported at the 1σ level. Isoplot application software was employed for data processing (Ludwig, 2001).

4. Geochronology

The cathodoluminescence (CL) imaging of zircon was completed at the Electron Microprobe Laboratory, Institute of Geology and Geophysics, Chinese Academy of Sciences (samples B14 and B231) and at the Beijing SHRIMP Centre (samples C270 and C134).

https://doi.org/10.1017/S0016756811000987 Published online by Cambridge University Press

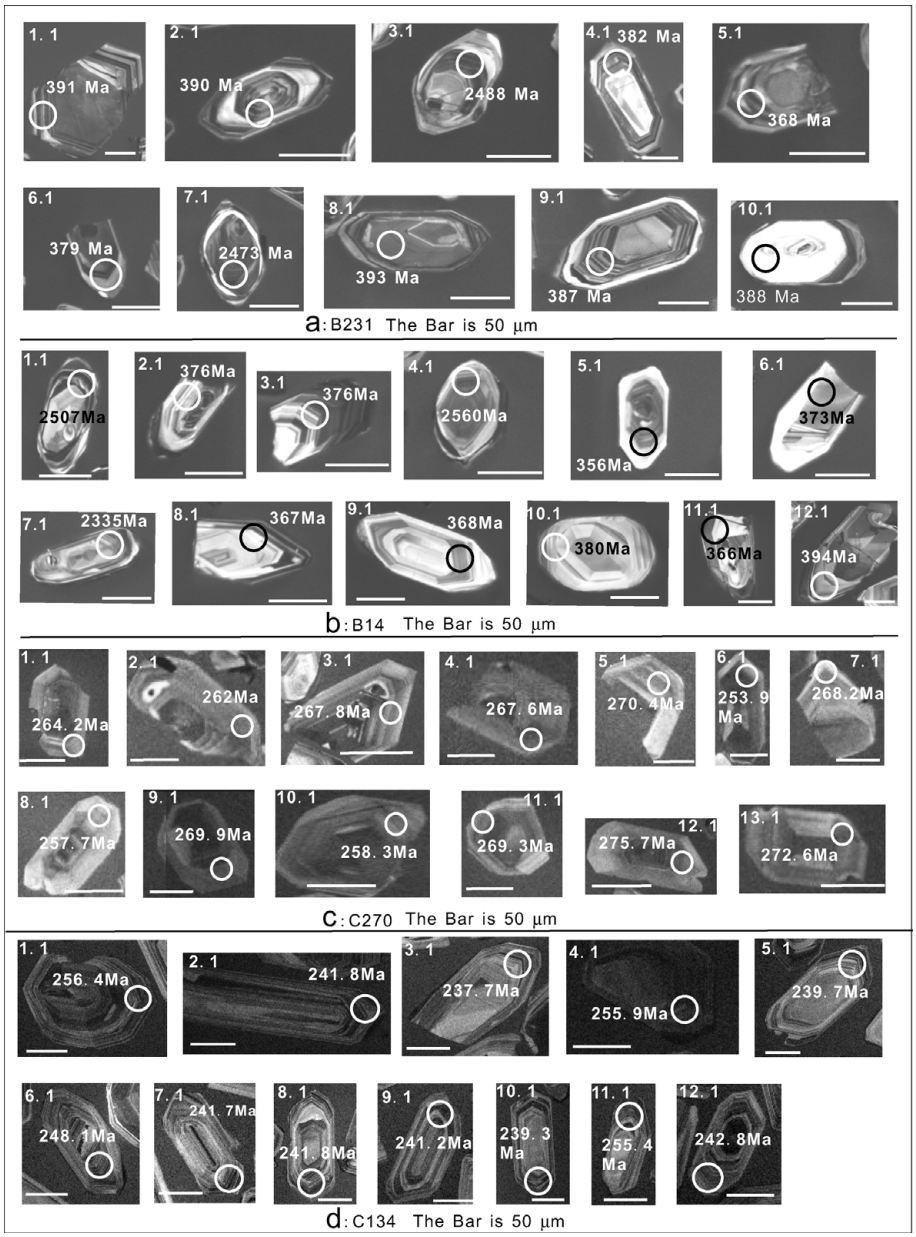

Figure 4. Cathodoluminescence (CL) images of zircons for Chehugou granitoids. (a) Porphyritic granite (B231); (b) fine granite (B14); (c) syenogranite (C270); (d) granite porphyry (C134).

All zircon grains have oscillating zones (Fig. 4), indicating a magmatic origin. The U–Pb isotopic data for the zircons are listed in Table 1 and shown in Figure 5. The errors of weighted mean ages are 2σ.

Zircon grains from the porphyritic monzogranite (B231) in the deposit area (Table 1) have U and Th contents of 85–886 ppm and 87–971 ppm, with Th/U ratios of 0.29–1.1, possibly indicating a magmatic origin. The common Pb was low in all of the ten analyses. Two grains out of the ten analyses have ancient ages (2488 and 2473 Ma), indicating an inherited origin. The other eight zircon grains are concordant with a weighted mean ^{206}Pb–^{238}U age of 384.7 ± 4.0 Ma (MSWD = 0.10). The age is interpreted to be the crystallization age of the porphyritic monzogranite.

Zircon grains from the syenogranite (B14) have U and Th contents of 82–609 ppm and Th = 14–1752 ppm, with Th/U ratios of 0.1–2.88. The common Pb content was low at all of the 12 analysis points. Three zircon grains out of the 12 analyses have ancient ages of 2335–2560 Ma, indicating an inherited origin. The other nine grains are concordant and yield a weighted mean ^{206}Pb–^{238}U age of 373.1 ± 5.9 Ma (MSWD = 1.4), indicating the emplacement age of the syenogranite.

Zircon grains from the syenogranite porphyry (C270) have U and Th contents of 187–552 ppm and 172–637 ppm, with Th/U ratios of 0.67–1.59. Thirteen analysis have an age range of 253.9 ± 6.2 to 275.7 ± 6.6 Ma, and give a weighted mean ^{206}Pb–^{238}U age of 265.6 ± 3.5 Ma (MSWD = 1.02). The mean age is interpreted as the time of crystallization of the syenogranite porphyry.

Zircon grains from the granite porphyry (C134) have U and Th concentrations of 144–758 ppm and 67–610 ppm, with Th/U ratios of 0.38–1.33, indicating

https://doi.org/10.1017/S0016756811000987 Published online by Cambridge University Press

Table 1. Zircon U–Pb SIMS and SHRIMP data for the Chehugou granitic complex intrusive rocks

Sample no	% $^{206}Pb_c$	U ppm	Th ppm	$^{232}Th/^{238}U$	$^{207}Pb^1/^{206}Pb$	±%	$^{207}Pb^2/^{235}U$	±%	$^{206}Pb^3/^{238}U$	±%	$^{206}Pb/^{238}U$ Age (Ma)
Syenogranite (B14)											
1.1	0.01	317	136	0.428	0.16683	2.37	10.93571	2.81	0.4754	1.51	2507.2 ± 31.5
2.1	0.09	489	394	0.806	0.05296	1.31	0.43886	1.99	0.0601	1.50	376.3 ± 5.5
3.1	0.01	609	1752	2.878	0.05512	1.19	0.45761	1.92	0.0602	1.51	376.9 ± 5.5
4.1	0.01	562	461	0.820	0.16730	0.37	11.24615	1.55	0.4875	1.50	2560 ± 31.8
5.1	0.12	356	246	0.690	0.05539	2.58	0.43357	3.02	0.0568	1.57	356 ± 5.4
6.1	0.02	441	219	0.495	0.05441	2.95	0.44682	3.31	0.0596	1.50	373 ± 5.4
7.1	0.00	384	207	0.539	0.16026	0.36	9.64534	1.57	0.4365	1.53	2335 ± 30.1
8.1	0.17	179	15	0.086	0.05494	2.91	0.44468	3.27	0.0587	1.51	367.7 ± 5.4
9.1	0.32	91	143	1.574	0.05725	4.80	0.46492	5.03	0.0589	1.52	368.9 ± 5.4
10.1	0.18	118	109	0.931	0.05370	3.41	0.44989	3.73	0.0608	1.50	380.2 ± 5.6
11.1	0.82	82	95	1.150	0.05441	4.39	0.43883	4.64	0.0585	1.50	366.5 ± 5.4
12.1	0.14	190	14	0.076	0.05616	2.17	0.48839	2.65	0.0631	1.52	394.3 ± 5.8
Monzogranite (B231)											
1.1	0.03	789	232	0.294	0.05417	1.33	0.46731	2.01	0.0626	1.51	391.2 ± 5.7
2.1	>1e6	523	490	0.937	0.05529	1.74	0.47654	2.30	0.0625	1.50	390.9 ± 5.7
3.1	0.00	743	214	0.288	0.16344	0.31	10.61659	1.53	0.4711	1.50	2488.4 ± 31.1
4.1	0.04	550	206	0.374	0.05367	1.33	0.45172	2.01	0.0610	1.51	382 ± 5.6
5.1	0.01	614	260	0.424	0.05454	1.13	0.44209	1.88	0.0588	1.50	368.3 ± 5.4
6.1	0.70	886	971	1.096	0.05445	1.43	0.45529	2.09	0.0606	1.52	379.5 ± 5.6
7.1	0.00	715	388	0.543	0.16689	0.71	10.76213	1.70	0.4677	1.54	2473.5 ± 31.7
8.1	0.10	418	389	0.933	0.05383	1.85	0.46682	2.38	0.0629	1.50	393.2 ± 5.7
9.1	>1e6	843	542	0.643	0.05477	0.95	0.46806	1.77	0.0620	1.50	387.6 ± 5.6
10.1	0.22	85	87	1.025	0.05379	3.56	0.46024	4.08	0.0621	1.99	388.1 ± 7.5
Syenogranite porphyry (C270)											
1.1	–	413	637	1.59	0.0542	3.0	0.31	3.8	0.04180	2.4	264.2 ± 6.3
2.1	0.96	449	383	0.88	0.0548	5.2	0.31	5.7	0.04150	2.4	262 ± 6.2
3.1	0.84	250	322	1.33	0.0514	7.3	0.30	8.0	0.04240	3.2	267.8 ± 8.4
4.1	0.29	266	172	0.67	0.0512	3.6	0.30	4.4	0.04240	2.4	267.6 ± 6.4
5.1	1.04	281	330	1.21	0.0524	7.4	0.31	7.8	0.04280	2.5	270.4 ± 6.6
6.1	–	187	201	1.11	0.0596	3.8	0.33	4.5	0.04017	2.5	253.9 ± 6.2
7.1	–	235	326	1.44	0.0577	3.0	0.34	3.9	0.04250	2.4	268.2 ± 6.4
8.1	–	351	451	1.33	0.0528	2.8	0.30	3.7	0.04079	2.4	257.7 ± 6.1
9.1	–	333	226	0.70	0.0551	2.7	0.33	3.6	0.04280	2.4	269.9 ± 6.4
10.1	–	552	615	1.15	0.0506	2.4	0.29	3.4	0.04090	2.5	258.3 ± 6.2
11.1	–	278	351	1.30	0.0564	2.8	0.33	3.7	0.04270	2.4	269.3 ± 6.4
12.1	–	280	316	1.16	0.0568	4.3	0.34	4.9	0.04370	2.4	275.7 ± 6.6
13.1	0.42	309	322	1.08	0.0467	7.5	0.28	7.9	0.04320	2.5	272.6 ± 6.7
Granite porphyry (C134)*											
1.1	0.36	758	530	0.72	0.0522	2.3	0.28	4.2	0.04060	2.4	256.4 ± 6.0
2.1	0.89	262	337	1.33	0.0532	3.4	0.24	6.8	0.03820	2.6	241.8 ± 6.2
3.1	1.02	144	67	0.48	0.0555	4.2	0.25	6.8	0.03760	2.5	237.7 ± 5.9
4.1	−0.03	605	366	0.62	0.0513	2.1	0.29	3.1	0.04050	2.4	255.9 ± 6.0
5.1	−0.05	197	142	0.74	0.0532	3.7	0.28	4.5	0.03790	2.5	239.7 ± 5.8
6.1	0.14	524	403	0.79	0.0535	2.2	0.28	3.4	0.03920	2.4	248.1 ± 5.8
7.1	0.39	710	385	0.56	0.0543	1.9	0.27	5.1	0.03820	2.4	241.7 ± 5.7
8.1	0.31	550	374	0.70	0.0544	2.1	0.27	3.5	0.03820	2.4	241.7 ± 5.7
9.1	0.32	385	213	0.57	0.0536	2.3	0.27	5.1	0.03810	2.4	241.2 ± 5.7
10.1	0.00	283	103	0.38	0.0533	4.5	0.28	5.2	0.03780	2.6	239.3 ± 6.1
11.1	−0.21	583	610	1.08	0.0526	2.0	0.30	3.1	0.04040	2.4	255.4 ± 5.9
12.1	0.37	357	200	0.58	0.0530	2.8	0.15	8.2	0.02420	2.5	242.8 ± 5.8

% $^{206}Pb_c$ denotes the percentage of ^{206}Pb that is common Pb.
[1]Common Pb corrected using measured ^{204}Pb.
[2]Common Pb corrected by assuming $^{206}Pb/^{238}U$–$^{207}Pb/^{235}U$ age-concordance.
[3]Common Pb corrected by assuming $^{206}Pb/^{238}U$–$^{208}Pb/^{232}Th$ age-concordance.
*Zeng *et al*. (2011*a*).

a magmatic origin. Twelve analyses give ages between 237.7 ± 5.9 and 256.4 ± 6.0 Ma. They plot on or near the concordia curve with a weighted mean ^{206}Pb–^{238}U age of 245.1 ± 4.4 Ma (MSWD = 1.4), indicating the crystallization age of the granite porphyry.

5. Geochemistry and Sr–Nd–Pb isotopic compositions

5.a. Major and trace elements

Major and trace element data for 11 rock samples, including two Devonian granite samples, three Permian syenogranite porphyry samples and six Triassic granite porphyry samples, from the Chehugou granitic complex are listed in Table 2.

The two Devonian granite samples have SiO_2 contents of 68.5–74.6 wt % and Al_2O_3 contents of 13.3–16.2 wt %, with K_2O/Na_2O ratios of 0.44–0.52. They are metaluminous to weakly peraluminous with A/CNK of 0.95–1.04 and belong to the calc-alkaline series of granitic rocks (Fig. 6a, b). Three Permian syenogranite porphyry samples have SiO_2 contents of 70.7–71.6 wt %, Al_2O_3 contents of 14.4–14.9 wt %, K_2O/Na_2O ratios of 1.13–1.25 and are alkali-calcic. Six

https://doi.org/10.1017/S0016756811000987 Published online by Cambridge University Press

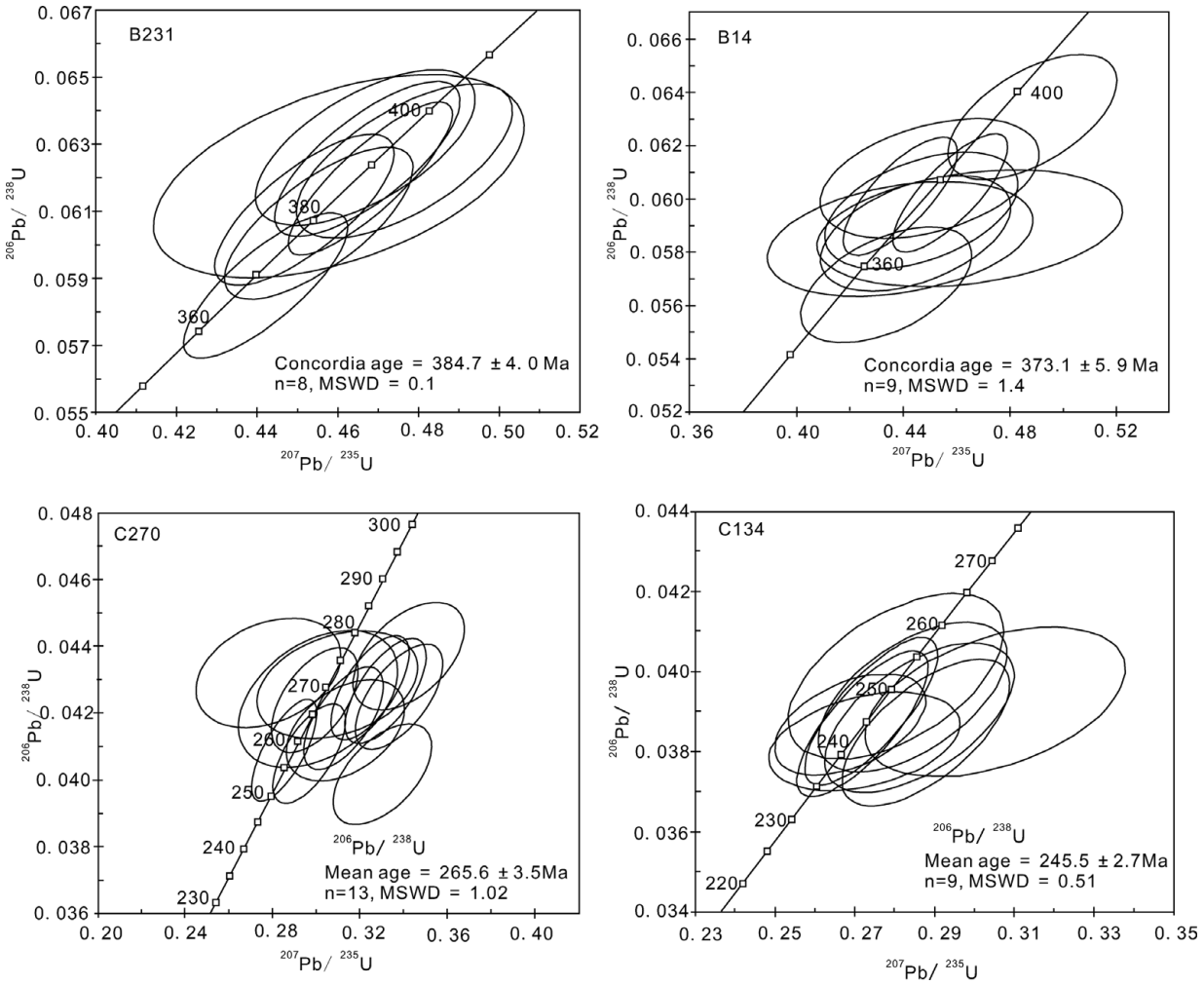

Figure 5. U–Pb zircon Concordia plots.

Triassic granite porphyry samples have SiO_2 contents of 70.3–74.0 wt %, Al_2O_3 contents of 13.3–15.1 wt % and K_2O/Na_2O ratios of 0.78–1.63. They belong to the calc-alkaline and alkali-calcic series of rocks (Fig. 6a). The Permian and Triassic granitoids are metaluminous to weakly peraluminous with A/CNK ratios of 0.96–1.10 (Fig. 6b).

The Devonian, Permian and Triassic granitoids are enriched in light REEs (LREEs) and depleted in heavy REEs (HREEs) (i.e. Yb = 0.27–0.48), with $(La/Yb)_{CN}$ values of 24–83. In the chondrite-normalized REE diagram (Fig. 7), they all show concave-up REE patterns with differentiation of light–heavy REEs without Eu anomalies, similar to those in the Archaean tonalite–trondhjemite–granodiorite (TTG) suite (Condie, 1993). They have Eu/Eu^* values of 0.9–1.2, 0.9–1.2 and 1.0–1.3 for the Devonian, Permian and Triassic granitoids, respectively.

The Devonian, Permian and Triassic granitoids have high Sr contents of 189–1256 ppm and low Y concentrations of 3.87–5.43 ppm, with Sr/Y ratios of 59–281. They are enriched in large-ion lithophile elements (LILEs), such as Rb, Sr, K and Th, and depleted in high-field-strength elements (HFSEs), such as Nb and Ta. In the primitive mantle-normalized trace element diagram (Fig. 8), they have strongly negative Nb and Ta anomalies and with generally positive Sr anomalies.

5.b. Sr–Nd–Pb isotopes

The Rb–Sr, Sm–Nd and Pb isotopic compositions of the Chehugou granitic complex are listed in Tables 3 and 4 and shown in Figures 9 and 10. The Devonian granites have relatively high initial $^{87}Sr/^{86}Sr$ ratios (0.7100–0.7126), and relatively homogeneous $^{143}Nd/^{144}Nd$ ratios (0.51166–0.51167), with $\varepsilon_{Nd}(t)$ values of −12.3 to −12.4. They have $^{206}Pb/^{204}Pb$, $^{207}Pb/^{204}Pb$ and $^{208}Pb/^{204}Pb$ ratios of 16.46–17.50, 15.32–15.46 and 37.61–38.40, respectively.

The Permian and Triassic granites have relatively low initial $^{87}Sr/^{86}Sr$ ratios (0.7048–0.7074), and heterogeneous $^{143}Nd/^{144}Nd$ ratios (0.51165–0.51180), with $\varepsilon_{Nd}(t)$ values of −13.1 to −10.1. They have $^{206}Pb/^{204}Pb$, $^{207}Pb/^{204}Pb$ and $^{208}Pb/^{204}Pb$ ratios of 17.23–17.51, 15.32–15.51 and 37.87–38.41, respectively.

The Chehugou granitoids have similar Sr–Nd isotopic compositions to the basement rocks of the NCC (Jahn *et al*. 1999) but are distinct from the Phanerozoic granites in the Central Asia Orogenic Belt (Wu, Sun

https://doi.org/10.1017/S0016756811000987 Published online by Cambridge University Press

Table 2. Major (wt %), rare earth and trace element (ppm) data for the Chehugou granitic complex intrusion

	Triassic granite porphyry						Permian syenogranite porphyry			Devonian granite	
Sample no.	C82	C232	C268	C349	C272	C346	C69	C202	C270	B14	B231
SiO_2 (wt %)	70.29	72.54	71.02	71.25	71.15	74.02	70.66	71.64	70.85	74.60	68.51
TiO_2	0.38	0.27	0.26	0.28	0.27	0.23	0.31	0.27	0.25	0.08	0.25
Al_2O_3	14.92	14.67	15.13	14.67	14.18	13.32	14.87	14.41	14.48	13.25	16.21
Fe_2O_3	1.35	1.21	1.45	1.16	1.56	1.74	1.50	1.21	1.57	0.59	2.27
MnO	0.01	0.01	0.01	0.01	0.01	0.01	0.01	0.01	0.01	0.01	0.05
MgO	0.54	0.47	0.50	0.64	0.49	0.49	0.61	0.54	0.54	0.19	0.64
CaO	1.65	1.09	1.41	1.26	1.79	1.08	1.40	1.55	1.18	0.38	2.52
Na_2O	4.42	4.38	4.86	3.36	3.95	3.71	4.12	3.92	4.09	6.22	4.94
K_2O	3.94	3.76	3.78	5.48	4.63	4.27	4.67	4.90	5.00	2.74	2.56
P_2O_5	0.17	0.09	0.08	0.10	0.10	0.09	0.11	0.10	0.08	0.02	0.10
LOI	2.32	1.74	1.70	1.20	2.10	1.32	1.06	1.60	1.34	1.42	1.46
Total	100.00	100.23	100.20	99.40	100.24	100.28	99.31	100.16	99.40	99.50	99.51
K_2O+Na_2O	8.36	8.14	8.64	8.84	8.58	7.98	8.79	8.82	9.09	8.96	7.50
K_2O/Na_2O	0.89	0.86	0.78	1.63	1.17	1.15	1.13	1.25	1.22	0.44	0.52
A/CNK	1.03	1.10	1.03	1.07	0.96	1.05	1.03	0.99	1.01	0.95	1.04
A/NK	1.29	1.30	1.25	1.28	1.23	1.24	1.27	1.23	1.19	1.00	1.48
Rb (ppm)	92	118	98	92	88	127	109	121	106	140	52
Sr	400	189	453	447	363	626	1256	728	461	318	1115
Zr	172	126	135	145	127	145	145	150	136	53	165
Nb	4.16	5.20	3.81	4.14	4.88	5.39	5.51	4.84	4.13	6.50	5.57
Cs	4.01	2.88	2.86	1.89	1.88	1.66	1.85	1.75	1.56	1.45	2.14
Ba	535	840	975	895	703	1912	930	772	1269	2111	1522
Y	5.20	5.30	4.05	3.87	4.50	4.64	4.46	4.38	4.90	5.43	5.37
La	27.3	22.0	25.8	27.3	22.8	24.5	31.2	33.8	38.3	15.8	34.3
Ce	53.9	38.4	45.2	48.1	41.3	43.1	56.9	58.5	59.4	26.7	59.1
Pr	6.34	3.89	4.83	5.10	4.44	4.48	6.16	6.08	6.01	3.07	6.37
Nd	22.7	13.2	16.0	16.7	15.1	14.7	21.2	19.8	19.6	9.9	19.9
Sm	3.55	2.00	2.48	2.43	2.26	2.11	2.91	2.92	3.00	1.80	3.11
Eu	0.84	0.57	0.75	0.61	0.74	0.59	0.85	0.78	0.64	0.45	0.90
Gd	2.29	1.48	1.72	1.76	1.54	1.57	2.03	1.97	2.14	1.33	2.15
Tb	0.24	0.18	0.19	0.20	0.17	0.17	0.20	0.20	0.22	0.18	0.24
Dy	1.06	0.89	0.78	0.87	0.71	0.77	0.83	0.86	1.01	0.89	0.93
Ho	0.18	0.16	0.12	0.16	0.12	0.14	0.14	0.14	0.17	0.17	0.17
Er	0.44	0.43	0.30	0.39	0.29	0.35	0.35	0.35	0.40	0.47	0.46
Tm	0.06	0.06	0.04	0.06	0.04	0.05	0.05	0.05	0.05	0.07	0.07
Yb	0.38	0.42	0.27	0.37	0.27	0.33	0.30	0.31	0.33	0.48	0.46
Lu	0.06	0.07	0.04	0.06	0.04	0.05	0.05	0.05	0.05	0.08	0.08
Hf	4.85	4.01	3.98	4.21	3.98	4.26	4.04	4.66	3.96	1.56	4.31
Ta	0.27	0.33	0.26	0.27	0.32	0.34	0.35	0.36	0.27	0.36	0.22
Pb	8.4	8.6	8.9	16.6	17.4	21.1	17.7	17.2	13.8	25.1	16.4
Th	7.04	8.49	5.95	7.27	7.83	7.83	6.86	10.38	6.08	5.02	5.01
U	1.86	2.92	1.91	2.19	2.34	2.25	1.51	2.34	2.06	0.45	0.32

A/CNK – Al/(Ca+Na+K) molar; A/NK – Al/(Na+K) molar; LOI – loss on ignition.

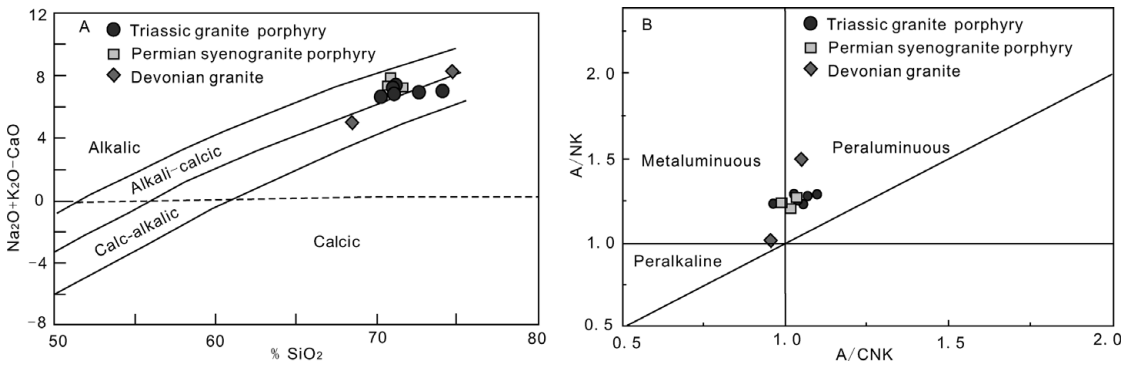

Figure 6. (a) Diagram of $Na_2O + K_2O - CaO$ versus SiO_2 (after Frost *et al*. 1976); (b) Diagram of A/NK versus A/CNK.

& Lin, 1999; Hong *et al*. 2000, 2003). Furthermore, they have similar Pb isotopic compositions to the host mafic rocks in the deposit, which have $^{206}Pb/^{204}Pb$, $^{207}Pb/^{204}Pb$ and $^{208}Pb/^{204}Pb$ ratios of 17.44, 15.50 and 38.36, respectively.

6. Discussion

6.a. Petrogenesis of the Chehugou granitoids

The Chehugou granitoids are characterized by relatively high silica and alkaline contents and low FeO

https://doi.org/10.1017/S0016756811000987 Published online by Cambridge University Press

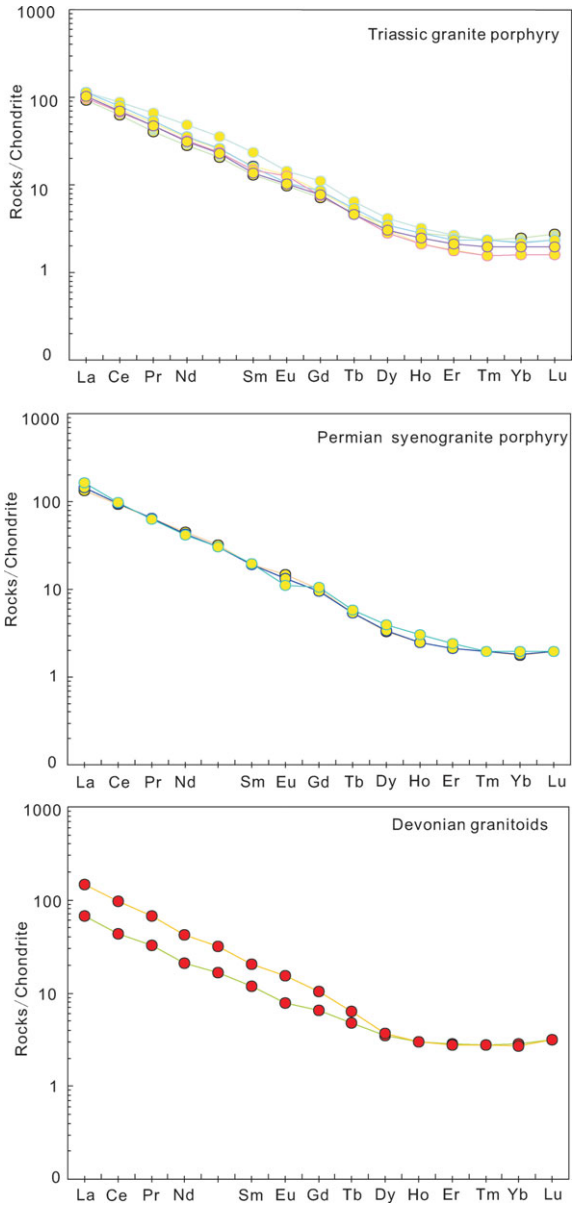

Figure 7. (Colour online) Chondrite-normalized REE patterns of the Chehugou granitic complex intrusion (normalization values after Boynton, 1984).

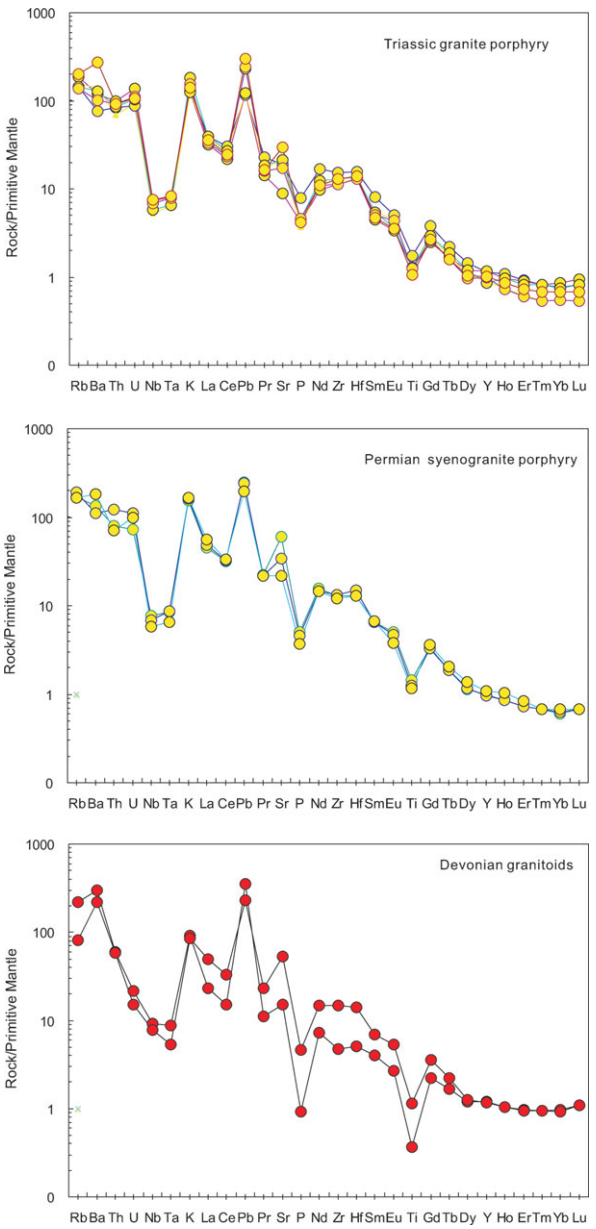

Figure 8. (Colour online) Primitive mantle-normalized trace elements web diagram of the Chehugou granitic complex intrusion (normalization values after Taylor & McLennan, 1985).

and MgO concentrations. They are calc-alkaline and alkali-calcic (Fig. 6a). They are enriched in LILEs, such as Rb, K, U and Th, and depleted in HFSEs, such as Nb, Ta, Ti and P. They have relatively high initial $^{87}Sr/^{86}Sr$ ratios of 0.7048–0.7126 and strongly negative $\varepsilon_{Nd}(t)$ (−10.1 to −13.1). Their ancient Nd model ages (1.5−2.69 Ga) (Table 3) are similar to the ages of the Palaeoproterozoic rocks in the northern NCC (Yang, *et al*. 2005; Zhang *et al*. 2007). All these geochemical features indicate that they were derived from partial melting of an ancient crustal source.

The Chehugou granitoids have relatively high Sr and Ba contents and low Y and Yb concentrations with high Sr/Y ratios. In the Sr/Y v. Y diagrams (Fig. 11), they plot in the field of adakites and TTG, far from the field of typical arc magmas. Furthermore, they have relatively high LREE concentrations and are depleted in HREEs, with $(La/Yb)_{CN}$ values of 24–83. All these geochemical features are similar to those of TTG/adakite and Na-rich granitoids in the world (e.g. Defant & Drummond, 1990; Atherton & Petford, 1993; Martin, 1999), which were suggested to be derived from partial melting of subducted oceanic crust or newly underplated lower crust under garnet stability conditions (e.g. Defant & Drummond, 1990; Atherton & Petford, 1993; Martin, 1999). Therefore, the Chehugou granites were derived from partial melting of ancient crustal materials at depth with garnet in stability, and with a plagioclase-poor and garnet-rich residual assemblage (Atherton & Petford, 1993; Patino Douce, 1999).

However, they have variable Nd isotopic compositions, indicating crustal assimilation and/or a mantle

https://doi.org/10.1017/S0016756811000987 Published online by Cambridge University Press

Table 3. The Sr–Nd isotopic data for the Chehugou granitic complex intrusive rocks

Sample	Lithology	Rb (ppm)	Sr (ppm)	$^{87}Rb/^{86}Sr$	$^{87}/^{86}Sr$	$^{87}/^{86}Sr$ (i)	Sm (ppm)
C206	TGP	140.422	295.661	1.3415	0.712025	0.707350	17.55
C268	TGP	98.023	452.939	0.6113	0.707640	0.705510	16.74
C272	TGP	92.251	447.419	0.5823	0.707562	0.705532	15.27
C349	TGP	126.723	626.123	0.5717	0.706793	0.704801	16.40
C270	PSP	105.569	461.074	0.6467	0.708569	0.706315	20.24
B363	PSP	107.775	205.158	1.4838	0.711292	0.705685	6.17
C69	PSP	109.240	1255.706	0.2457	0.707631	0.706775	19.66
C202	PSP	120.906	727.874	0.4691	0.708256	0.706621	19.75
B231	DG	106.093	37.655	7.9582	0.740026	0.709955	11.52
B14	DG	97.260	99.231	2.7684	0.723062	0.712601	9.72

Sample	Nd (ppm)	$^{147}Sm/^{144}Nd$	$^{143}Nd/^{144}Nd$	$(^{143}Nd/^{144}Nd)I$	εNd (*t*)	∫Sm/Nd	TDM1
C206	35.32	0.315251	0.512155	0.511649	−13.14	−0.603	1.50
C268	35.00	0.303450	0.512224	0.511737	−11.42	−0.543	1.58
C272	32.92	0.294293	0.512275	0.511803	−10.14	−0.496	1.67
C349	36.53	0.284836	0.512123	0.511666	−12.81	−0.448	2.22
C270	42.89	0.299402	0.512208	0.511728	−11.61	−0.522	1.69
B363	40.00	0.097773	0.511943	0.511773	−10.21	−0.503	1.59
C69	46.27	0.269578	0.512172	0.511740	−11.38	−0.371	2.69
C202	43.24	0.289789	0.512152	0.511687	−12.40	−0.473	2.01
B231	96.33	0.075875	0.511797	0.511665	−12.32	−0.614	1.50
B14	75.80	0.813590	0.511802	0.511661	−12.40	−0.586	1.55

TGP – Triassic granite porphyry; PSP – Permian syenogranite porphyry; DG – Devonian granite.

Table 4. Whole-rock Pb isotope data for the granitoids and mafic rocks in the Chehugou ore area

Sample no.	Sample description	$^{206}Pb/^{204}Pb$	2σ	$^{207}Pb/^{204}Pb$	2σ	$^{208}Pb/^{204}Pb$	2σ
C206	Triassic granite porphyry	17.320	0.018	15.506	0.017	38.093	0.016
C272	Triassic granite porphyry	17.514	0.007	15.479	0.008	38.409	0.008
C349	Triassic granite porphyry	17.287	0.019	15.329	0.018	38.284	0.019
B363	Permian syenogranite porphyry	17.229	0.018	15.427	0.022	37.870	0.028
C270	Permian syenogranite porphyry	17.450	0.017	15.450	0.017	38.217	0.016
B344	Permian syenogranite porphyry	17.483	0.023	15.437	0.023	38.271	0.024
B365	Permian syenogranite porphyry	17.315	0.016	15.418	0.020	37.962	0.019
B14	Devonian monzogranite	17.289	0.018	15.464	0.017	37.957	0.017
B231	Devonian syenogranite	16.458	0.038	15.315	0.037	37.607	0.049
B354	Devonian monzogranite	17.497	0.018	15.444	0.019	38.404	0.019
B373	Devonian monzogranite	16.839	0.014	15.346	0.018	37.940	0.015
B375	Devonian monzogranite	17.278	0.018	15.379	0.019	37.855	0.017
B35	Archaean plagioclase hornblende gneiss	17.436	0.023	15.504	0.023	38.360	0.022

material addition process. The occurrence of ancient zircons in the dated samples possibly indicates a crustal assimilation of the parental magmas of the Chehugou granitoids. However, the Chehugou granites contain plenty of microgranular enclaves. They mostly range from angular to oval in shape, but locally form dyke-like trails that progressively thin toward their terminations with the host granitoid. They range in composition from diorite to quartz diorite. Igneous textures include oscillatory-zoned plagioclase, local quartz and K-feldspar megacrysts and some myrmekitic intergrowths between plagioclase and alkali feldspar, identical to textures described from mafic enclaves around the world (Eichelberger 1980; Vernon, 1984; Holden *et al*. 1987; Vernon *et al*. 1988; Didier & Barbarin, 1991; Yang *et al*. 2004), indicating a magma mixing process in the origin of the Chehugou granites. Moreover, the mafic enclaves and host granites have similar Pb isotopic compositions, and plot between the lower crust and mantle lines of the $^{207}Pb/^{204}Pb$ v. $^{206}Pb/^{204}Pb$ diagram of Zartman & Doe (1981) (Fig. 10), indicating at least two components (lower crust and mantle) involved in the origin of the Chehugou granitoids.

Therefore, the whole-rock geochemical features and Sr–Nd–Pb isotopic compositions indicate that the Chehugou granitoids were mainly derived from partial melting of ancient crustal materials with garnet in the residues at high pressures, with crustal assimilation. Mafic enclaves can be considered to represent remnants of a mafic component added to intermediate to felsic magma chambers, indicating that the mantle-derived magmas provide heat and materials in the origin of the Chehugou granitoids.

6.b. Genetic relationship between the granites and Mo mineralization

It is well accepted that porphyry Cu and Cu–Mo deposits have genetic relationships with the petrogenesis of porphyritic granites. Porphyry Cu and Cu–Mo deposits are associated with intermediate to felsic, calc-alkaline intrusive rocks that range from granodiorite to granite

https://doi.org/10.1017/S0016756811000987 Published online by Cambridge University Press

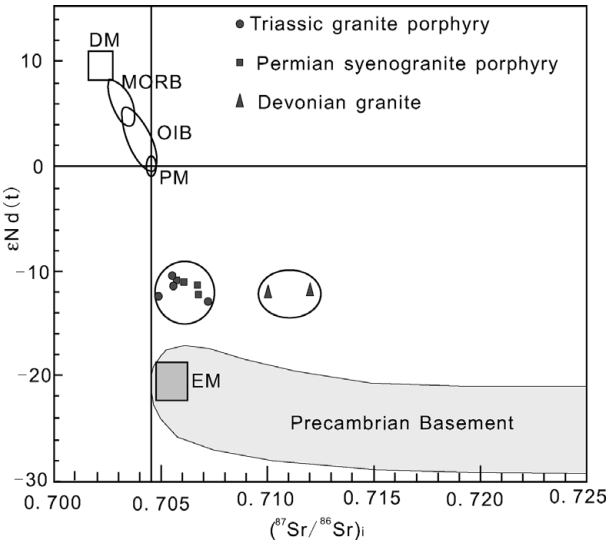

Figure 9. Diagram of initial Sr versus $\varepsilon_{Nd}(t)$ of the Chehugou granitic complex intrusion. Depleted mantle (DM), mid-ocean ridge basalt (MORB), ocean island basalt (OIB), primitive mantle (PM) and enriched mantle (EM) are defined by Hart (1984) and Zindler & Hart (1986). Precambrian basement is from Wu *et al*. (2005).

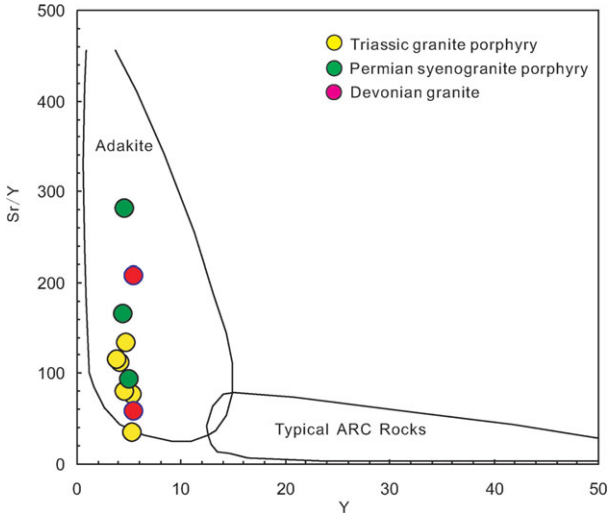

Figure 11. (Colour online) Sr/Y versus Y diagram for granitoids in Chehugou ore area.

in composition (60−72 wt % SiO_2) (Kesler, Jones & Walker, 1975; Titley & Beane, 1981). Porphyry Mo deposits, in comparison, are typically associated with felsic, high-silica (72−77 wt % SiO_2) and, in many cases, strongly differentiated granitic plutons (Mutschler *et al*. 1981; White *et al*. 1981; Kooiman, McLeod & Sinclair, 1986). Subduction-related calc-alkaline rocks are related to the Endako-type Mo deposit (or arc-type), and alkaline rocks are related to the Climax-type Mo deposit (rift-type) (Sillitoe, 1980; Carten, White & Stein, 1993). Subduction-related Chehugou granitoids belong to the calc-alkaline and alkali-calcic series of rocks, so it is favourable to form Endako-type Mo deposits (granitic porphyry Mo deposits) in the Chehugou complex.

In the Chehugou area, field observations show that the Mo orebodies spatially occur within the granite porphyry (Fig. 2). The Mo mineralization at Chehugou is predominantly localized in the Triassic granite porphyry stock. Stockwork and breccia mineralizations are recognized in the ore area. Stockwork veins (0.2 to 2 cm wide) include quartz, quartz-sulphide and sulphide veins that have narrow sericite envelopes. The stockwork mineralization is characterized by dissemination and veinlets of pyrite, molybdenite and chalcopyrite. Breccia mineralization occurs within a steep cryptoexplosive breccia pipe. Hydrothermally cemented breccias are spatially associated with higher ore grades than nearby veinlet-related mineralization. Ore minerals form part of the cement in these breccias. Widespread kaolinization, approximately round in shape in plan view, is recognized at Chehugou (Zeng *et al*. 2011*b*). The sericitization and silicification zone, associated with the stockwork and breccia ores, is under the kaolinization zone. Chehugou Mo deposits can be classified as granitic porphyry Mo deposits according to the classification scheme (Seedorff *et al*. 2005). Comparing the well-known Endako Mo deposit in British Columbia, Canada (Selby *et al*. 2000) with the Chehugou Mo deposit, we found that the Endako and

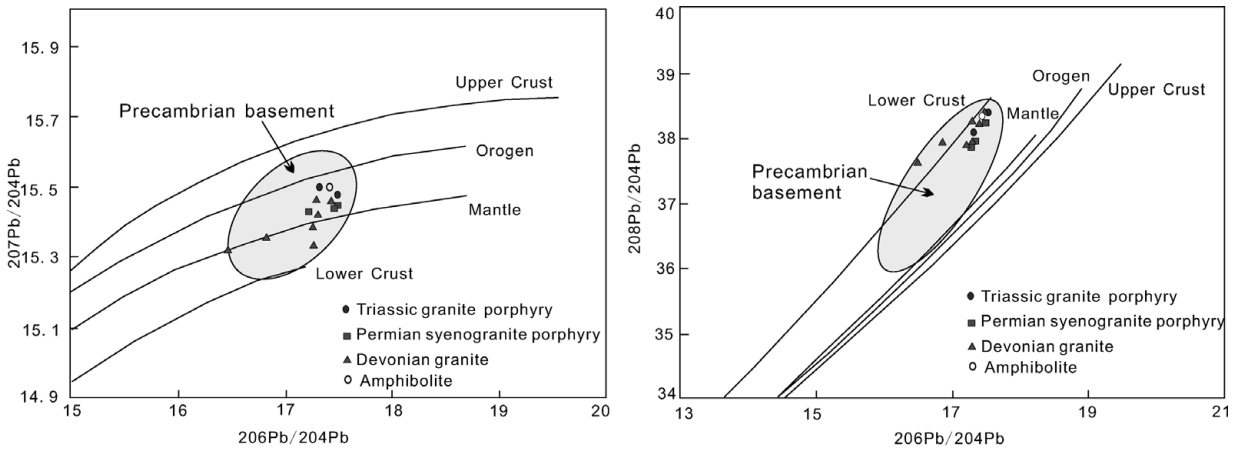

Figure 10. Diagram of Pb isotopic composition of the Chehugou wall rock Pb on the growth curves of Zartman & Doe (1981). Data for Precambrian basement are from Chen *et al*. (1994) and Li & Wang (1995).

https://doi.org/10.1017/S0016756811000987 Published online by Cambridge University Press

Chehugou Mo deposits belong to the same deposit type, but there are interesting differences between them. For example, three episodes of mineralization are related to three episodes of granitoid intrusion in the Endako deposit, but Mo mineralization in the Chehugou deposit is related to the last granite porphyry intrusion.

The excellent correlation between the Re–Os date from molybdenite and the ages of the granite porphyry from the area indicate a direct genetic relationship between the granite porphyry intrusion and Mo mineralization. The Re−Os isochron age for molybdenite is 245 ± 5 Ma (Zeng *et al*. 2011*a*), and the zircon U−Pb age of the granite porphyry is 245.1 ± 4.4 Ma. $\delta^{34}S$ values of sulphide from the Chehugou deposit range from −0.61 ‰ to 0.86 ‰ (Zeng *et al*. 2011*b*). The $\delta^{34}S$ values of sulphide are similar to the $\delta^{34}S$ values of typical magmatic sulphide sulphur (Ohmoto, 1986), suggesting that the ore-forming materials are magmatic in origin. Geochemical features suggest that the Devonian, Permian and Triassic Chehugou granitoids were mainly derived from partial melting of ancient crustal materials with garnet in the residues at high pressures, with minor involvement of a mantle component and crustal assimilation. Therefore, we infer that the Mo is derived from the ancient crustal rocks and that the minor Cu is derived from the mantle. This result is consistent with the study of the source region of metals in porphyry deposits (Candela & Piccoli, 2005; Seedorff *et al*. 2005).

The monzogranite, syenogranite and syenogranite porphyry in the Chehugou deposit have crystallization ages of 373.1 ± 5.9 Ma, 384.7 ± 4.0 Ma and 265.6 ± 3.5 Ma, respectively. Furthermore, the Devonian granites have distinct initial $^{87}Sr/^{86}Sr$ ratios from the Permian and Triassic granitoids in the Chehugou granitic batholith, indicating a different source. Although the Mo deposits are hosted by granitoids, there is no genetic relationship between the Mo mineralization and the Devonian and Permian granites in the Chehugou deposit.

6.c. Tectonic implications

The northern margin of the NCC and southern margin of the Siberian Craton underwent Andean-type magmatism in Late Palaeozoic time. The presence of both northward- and southward-facing active continental margins in Permian time suggests that the Palaeo-Asian Ocean closed at this time by subduction in two directions (Xiao *et al*. 2003). Many studies show that the collision between the Siberian plate and the North China plate ceased at the end of the Permian period (Dobretsov, Berzin & Buslov, 1995; Windley *et al*. 2002; Xiao *et al*. 2003; Wu *et al*. 2007). The emplacement age (244 Ma) of the Hegenshan ophiolite (Miao *et al*. 2008), a series of post-collision granites (Shi *et al*. 2004), mafic–ultramafic rocks (Wu *et al*. 2004), the Permian radiolarians (Shang, 2004) and a syncollision granite (248 Ma) (Wu *et al*. 2007) indicate that the tectonic setting of the northern margin of NCC is a syncollision setting in Early Triassic time.

The Chehugou granitoids have strongly negative $\varepsilon_{Nd}(t)$ values (−13.14 to −10.14), distinct from those of Phanerozoic granites in the Central Asian Orogenic Belt (−2.2 to +7.1; Wu, Sun & Lin, 1999; Hong *et al*. 2000) on the northern side of the deposit area, but similar to those of Phanerozoic granites in the northern NCC (Zhang *et al*. 2007), indicating that the Chehugou deposit is likely located in the northern NCC.

The Chehugou granitic complex mainly consists of monzogranite, syenogranite, syenogranite porphyry and granite porphyry. The geochemical features of the granitoids indicate that the Devonian granite belongs to the calc-alkaline rock series, the Permian syenogranite porphyry belongs to the alkali-calcic rock series and the Triassic granite porphyry belongs to the calc-alkaline and alkali-calcic rock series. The calc-alkaline rocks are generally formed in subduction zones related to arc-continent or continental collision (Barbarin, 1999). So, the Chehugou granitoids were formed in a subduction zone related to arc-continent or continental collision between the North China and Siberian plates. The Devonian granites are sodic with relatively low K_2O/Na_2O ratios, similar to the geochemical features of continental arc magmatism and may be formed within a subduction zone and related to the closure of the Palaeo-Asian Ocean. The Permian and Triassic granitoids have geochemical features of syn- or post-orogenic magmatism (Batchelor & Bowden, 1985). The trace element spider diagram shows enrichment in LILEs, impoverishment in HFSEs and depletions of Nb, Ta, P and Ti, all indicative of the trace element features of postcollision calc-alkaline and alkali-calcic I-type granite (Kuster & Harms, 1998; Xiao, Deng & Ma, 2002). The data suggest that all of the granitoids of the Chehugou batholith, regardless of age, were formed within a compressional tectonic setting. The formation of the granitic rocks is likely related to subduction of the Palaeo-Asian Ocean and subsequent collision between the Siberian and North China blocks.

The Devonian (384–373 Ma) granite reflects the southward subduction of the Palaeo-Asian Ocean plate, whereas the Permian (265 Ma) syenogranite porphyry and Triassic (245 Ma) granite porphyry indicate that the Palaeo-Asian Ocean was closed during the Late Permian period, and subsequent continent–continent collision occurred after the closure of the Palaeo-Asian Ocean during the Early Triassic period. Therefore, the Devonian, Permian and Triassic granites on the northern margin of the NCC were formed by partial melting of the North China Block during the period of subduction and continental collision between the North China and Siberian plates (Fig. 12a, b).

7. Conclusions

(1) The Chehugou granitic complex is composed of monzogranite, syenogranite, syenogranite porphyry and granite porphyry, with the former two belonging to

https://doi.org/10.1017/S0016756811000987 Published online by Cambridge University Press

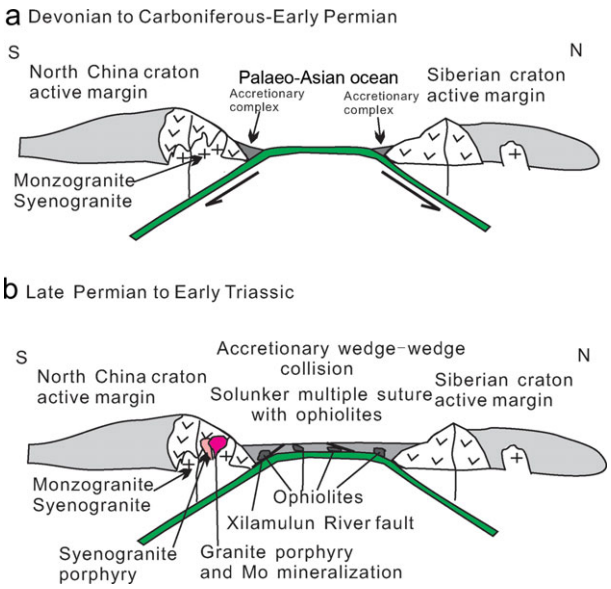

Figure 12. (Colour online) Schematic cartoons showing the Devonian to Triassic evolution of the northern margin of North China Craton (modified from Xiao *et al*. 2003). (a) Devonian–Early Permian: two-way subduction of Palaeo-Asian Ocean plate; (b) Late Permian–Early Triassic: syncollision-related porphyritic stocks and formation of porphyry-related Mo mineralization.

a calc-alkaline rock series, the syenogranite porphyry belonging to the alkali-calcic rock series and the granite porphyry belonging to the calc-alkaline and alkali-calcic rock series.

(2) The granitoids yield SIMS U–Pb zircon ages of 384.7 ± 4.0 Ma for the monzogranite and 373.1 ± 5.9 Ma for the syenogranite, and the SHRIMP U–Pb zircon ages are 265.6 ± 3.5 Ma for the syenogranite porphyry and 245.1 ± 4.4 Ma for the granite porphyry; the metallogenesis relates to the Triassic granite porphyry.

(3) The Devonian to Triassic granite on the northern margin of the NCC was formed by partial melting of the North China Block during the period of subduction and continental collision between the North China and Siberian plates.

Acknowledgements. We sincerely thank the following organizations and people for their support and help: Chifeng Chehugou Molybdenum Mine, which greatly supported our field work; Dr Liu Jianhui from the Ion Microprobe Centre, Institute of Geology, Chinese Academy of Geological Sciences, who helped us with the SHRIMP U–Pb zircon dating test; senior engineer Li He from the Rock and Mineral Analysis Laboratory, Institute of Geology and Geophysics, Chinese Academy of Sciences, who helped with our major element analysis of rocks; researcher Jin Xindi from the Trace Element Analysis Laboratory, Institute of Geology and Geophysics, Chinese Academy of Sciences, who helped us with the trace and rare earth element analysis of the rocks; and Dr Chu Zhuoyin from the Laboratory for Radiogenic Isotope Geochemistry, Institute of Geology and Geophysics, Chinese Academy of Sciences, who provided help with our Pb isotope analysis. We thank J. Gregory Shellnutt, Zhu Laimin, Clive Rice and an anonymous reviewer for their detailed comments. We specially thank Dr Phil Leat, journal editor, for his constructive comments and help. This work was financially supported by the National Natural Science Foundation of China (No. 40972065) and the Special Study Programme of the Continuous Resources of Crisis Mine of China (No. 20089931).

References

ATHERTON, M. P. & PETFORD, N. 1993. Generation of sodium-rich magmas from newly underplated basaltic crust. *Nature* **362**, 144–6.

BARBARIN, B. 1999. A review of the relationships between granitoid types, their origins and their geodynamic environments. *Lithos* **46**, 605–26.

BATCHELOR, R. A. & BOWDEN, P. 1985. Petrogenetic interpretation of granitoid rock series using multicationic parameters. *Chemical Geology* **48**, 43–55.

BLACK, L. P., KAMO, S. L., ALEIIKOF, J. N., DAVIS, D. W., KORSCH, R. L. & FOUDOULIS, C. 2003. TEMORA 1: a new zircon standard for Phanerozoic U–Pb geochronology. *Chemical Geology* **200**, 155–70.

BOYNTON, W. V. 1984. Cosmochemistry of rare earth elements: meteorite studies. In *Rare Earth Element Geochemistry* (ed. P. Henderson), pp. 63–114. Amsterdam: Elsevier.

BUREAU OF GEOLOGY AND MINERAL RESOURCES OF NEIMONGOL AUTONOMOUS REGION (BGMR). 1991. *Regional Geology of Neimongol Autonomous Region*. Beijing: Geological Publishing House, 532 pp. (in Chinese).

CANDELA, P. A. & PICCOLI, P. 2005. Magmatic processes in the development of porphyry-type ore systems. In *Economic Geology, 100th Anniversary Volume* (eds J. W. Hedenquist, J. F. H. Thompson, R. J. Goldfarb & J. P. Richards), pp. 25–37. Littleton, Colorado: Society of Economic Geologists.

CARTEN, R. B., WHITE, W. H. & STEIN, H. J. 1993. High-grade granite-related molybdenum systems: classification and origin. In *Mineral Deposit Modelling* (eds R. V. Kirkham, W. D. Sinclair, R. I. Thorpe & J. M. Duke), pp. 521–44. Geological Association of Canada, Special Paper no. 40.

CHEN, F. K., HEGNER, E. & TODT, W. 2000. Zircon ages, Nd isotopic and chemical compositions of orthogneisses from the Black Forest, Germany – evidence for a Cambrian magmatic arc. *International Journal of Earth Sciences* **88**, 791–802.

CHEN, W. J., LIU, J. M., LIU, H. T., ZHANG, Z. L., QIN, F. & ZHANG, R. B. 2010. Geochronology and fluid study of the Jiguanshan porphyry Mo deposit, Inner Mongolia. *Acta Petrologica Sinica* **26**, 1423–36 (in Chinese with English abstract).

CHEN, F. K., SIEBEL, W., SATIR, M., TERZIOGLU, N. & SAKA, K. 2002. Geochronology of the Karadere basement (NW Turkey) and implications for the geological evolution of the Istanbul zone. *International Journal of Earth Sciences* **91**, 469–81.

CHEN, Z. S., ZHANG, L. G., LIU, J. X., WANG, B. C., XU, J. F. & ZHENG, W. S. 1994. A study on lead isotope geochemical backgrounds of geological bodies in Jiaodong region. *Contributions to Geology and Mineral Resources Research* **10**, 65–78 (in Chinese with English abstract).

CONDIE, K. C. 1993. Chemical composition and evolution of the upper continental crust: contrasting results from surface samples and shales. *Chemical Geology* **104**, 1–37.

DEFANT, M. J. & DRUMMOND, M. S. 1990. Derivation of some modern arc magmas by melting of young subducted lithosphere. *Nature* **347**, 662–5.

DIDIER, J. & BARBARIN, B. 1991. *Enclaves and Granite Petrology. Developments in Petrology 13*. Amsterdam: Elsevier, 625 pp.

DOBRETSOV, N. L., BERZIN, N. A. & BUSLOV, M. 1995. Opening and tectonic evolution of the Paleo-Asian Ocean. *International Geology Review* **37**, 335–60.

EICHELBERGER, J. C. 1980. Vesiculation of mafic magma during replenishment of silicic magma reservoirs. *Nature* **288**, 446–50.

FROST, B. R., BARNES, C. G., COLLINS, W. J., ARGULUS, R. J., ELLIS, D. J. & FROST, C. D. 2001. A geochemical classification for granitic rocks. *Journal of Petrology* **42**, 2033–48.

GAO, S., LIU, X. M., YUAN, H. L., HATTENDORF, B., GUNTHER, D., CHEN, L., & HU, S. H. 2002. Determination of forty-two major and trace elements in USGS and NIST SRM glasses by laser ablation-inductively coupled plasma-mass spectrometry. *Geostandards Newsletter* **26**, 191–6.

HART, S. R. 1984. A large-scale isotope anomaly in the Southern Hemisphere mantle. *Nature* **309**, 753–7.

HOLDEN, P., HALLIDAY, A. N. & STEPHENS, W. E. 1987. Neodymium and strontium isotope content of microdiorite enclaves points to mantle input to granitoid production. *Nature* **330**, 53–6.

HONG, D. W., WANG, S. G., XIE, X. L. & ZHANG, J. S. 2000. Genesis of positive $\varepsilon_{Nd}(t)$ granitoids in Da Hinggan Mountains–Mongolia orogenic belt and growth of continental crust. *Earth Science Frontiers* **7**, 441–56 (in Chinese with English abstract).

HONG, D. W., WANG, S. G., XIE, X. L., ZHANG, J. S. & WANG, T. 2003. Correlation between continental growth and the supercontinental cycle: evidence from the granites with positive ε_{Nd} in the Central Asian orogenic belt. *Acta Geologica Sinica* **77**, 203–9 (in Chinese with English abstract).

JAHN, B. M., WU, F. Y., LO, C. H. & TSAI, C. 1999. Crust-mantle interaction induced by deep subduction of the continental crust: geochemical and Sr–Nd isotopic evidence from post-collisional mafic-ultramafic intrusions of the northern Dabie complex, central China. *Chemical Geology* **157**, 119–46.

KESLER, S. E., JONES, L. M. & WALKER, R. L. 1975. Intrusive rocks associated with porphyry copper mineralization in island arc areas. *Economic Geology* **70**, 515–26.

KOOIMAN, G. J. A., MCLEOD, M. J. & SINCLAIR, W. D. 1986. Porphyry tungsten-molybdenum orebodies, polymetallic veins and replacement bodies, and tin-bearing greisen zones in the Fire Tower Zone, Mount Pleasant, New Brunswick. *Economic Geology* **81**, 1356–73.

KUSTER, D. & HARMS, U. 1998. Post-collisional potassic granitoids from the southern and northwestern parts of the late Neo-proterozoic East African Orogen: a review. *Lithos* **45**, 177–95.

LI, X. H., LIU, Y., LI, Q. L., GUO, C. H. & CHAMBERLAIN, K. R. 2009. Precise determination of Phanerozoic zircon Pb/Pb age by multicollector SIMS without external standardization. *Geochemistry Geophysics Geosystems* **10**, Q04010, doi:10.1029/2009GC002400, 21 pp.

LI, S. C. & WANG, S. L. 1995. Geochemical characteristics of gold deposits of the north margin of the North China Continental Table, China. *Contributions to Geology and Mineral Resources Research* **10**, 8–19 (in Chinese with English abstract).

LIU, J. M., ZHAO, Y., SUN, Y. L., LI, D. P., LIU, J., CHEN, B. L., ZHANG, S. H. & SUN, W. D. 2010. Recognition of the latest Permian to Early Triassic Cu–Mo mineralization on the northern margin of the North China block and its geological significance. *Gondwana Research* **17**, 125–34.

Ludwig K. R. 2001. *Users Manual for Isoplot/Ex Rev. 2.49*. Berkeley Geochronology Centre Special Publication no. 1a, 56 pp.

MARTIN, H. 1999. Adakitic magma: modern analogues of Archean granitoids. *Lithos* **46**, 411–29.

MIAO, L. C., FAN, W. M., LIU, D. Y., ZHANG, F. Q., SHI, Y. R. & GUO, F. 2008. Geochronology and geochemistry of the Hegenshan ophiolitic complex: implications for late-stage tectonic evolution of the Inner Mongolia-Daxinganling Orogenic Belt, China. *Journal of Asian Earth Sciences* **32**, 348–70.

MUTSCHLER, F. E., WRIGHT, E. G., LUDINGTON, S. & ABBOTT, J. T. 1981. Granite molybdenite systems. *Economic Geology* **76**, 874–97.

NIE, F. J., ZHANG, W. Y., DU, A. D., JIANG, S. H. & LIU, Y. 2007. Re-Os isotopic dating on molybdenite separates from the Xiaodonggou porphyry Mo deposit, Hexigten Qi, Mongolia. *Acta Geologica Sinica* **81**, 898–905 (in Chinese with English abstract).

OHMOTO, H. 1986. Stable isotope geochemistry of ore deposits. In *Reviews in Mineralogy vol. 16: Stable Isotopes in High Temperature Geological Processes* (eds J. W. Valley, H. P. Taylor & J. R. O'Neil), pp.491–559. Mineralogical Society of America.

PATINO DOUCE, A. E. 1999. What do experiments tell us about the relative contribution of crust and mantle to the origin of granitic magmas? In *Understanding Granites: Integrating New and Classical Techniques* (eds A. Castro, C. Fernández & J. L. Vignersse), pp. 55–76. Geological Society of London, Special Publication no. 168.

QIN, F., LIU, J. M., ZENG, Q. D. & LUO, Z. H. 2009. Petrogenetic and metallogenic mechanism of the Xiaodonggou porphyry molybdenum deposit in Hexigten Banner, Inner Mongolia. *Acta Petrologica Sinica* **25**, 3357–68 (in Chinese with English abstract).

RUI, Z. Y., SHI, L. D. & FANG, R. L. 1994. *Geology and Nonferrous Metallic Deposits in the Northern Margin of the North China Landmass and its Adjacent Area*. Beijing: Geological Publishing House, 476 pp. (in Chinese).

SEEDORFF, E., DILLES, J. H., PROFFETT, JR, J. M. & EINAUDI, M. T. 2005. Porphyry deposits: characteristics and origin of hypogene features. *Economic Geology, 100th Anniversary Volume* (eds J. W. Hedenquist, J. F. H. Thompson, R. J. Goldfarb & J. P. Richards), pp. 251–98. Littleton, Colorado: Society of Economic Geologists.

SELBY, D., NESBITT, B. E., MUEHLENBACHS, K. & PROCHASKA, W. 2000. Hydrothermal alteration and fluid chemistry of the Endako porphyry molybdenum deposit, British Columbia. *Economic Geology* **95**, 183–202.

SHANG, Q. H. 2004. The discovery of the Permian radiolarian in Middle-Eastern Inner Mongolia, North China Orogenic Belt, and its significance. *Chinese Science Bulletin* **49**, 2574–9 (in Chinese).

SHI, G. H., MIAO, L. C., ZHANG, F. Q., JIAN, P., FAN, W. M. & LIU, D. Y. 2004. The time of A-type granite of Xilinhaote, Inner Mongolia, and its tectonic significance. *Chinese Science Bulletin* **49**, 384–9 (in Chinese).

SILLITOE, R. H. 1980. Types of porphyry molybdenum deposits. *Mining Magazine* **142**, 550–3.

SLÁMA, J., KOLER, J., CONDON, D. J., CROWLEY, J. L., GERDES, A., HANCHAR, J. M., HORSTWOOD, M. S. A., MORRIS, G. A., NASDALA, L., NORBERG, N., SCHALTEGGER, U., SCHOENE, B., TUBRETT, M. N. & WHITEHOUSE, M. J. 2008. Plesovice zircon—A new natural reference material for U-Pb and Hf isotopic microanalysis. *Chemical Geology* **249**, 1–35.

SONG, B., ZHANG, Y. & WAN, Y. S. 2002 Mount making and procedure of the SHRIMP dating. *Geological Review* **48(Supp)**, 26–30 (in Chinese).

STACEY, J. S. & KRAMERS, J. D. 1975. Approximation of terrestrial lead isotope evolution by a two-stage model. *Earth and Planetary Science Letters* **26**, 207–21.

TAYLOR, S. R. & MCLENNAN, S. M. 1985. *The Continental Crust: Its Composition and Evolution*. Oxford: Blackwell Scientific Publications, 312 pp.

TITLEY, S. R. & BEANE, R. E. 1981. Porphyry copper deposits. In *Economic Geology Seventy-Fifth Anniversary Volume, 1905–1980* (ed. B. J. Skinner), pp. 214–69. Economic Geology Publishing Co.

VERNON, R. H. 1984. Microgranitoid enclaves in granite-globules of hybrid magma quenched in a plutonic environment. *Nature* **309**, 438–9.

VERNON, R. H. & FLOOD, R. H. 1988. Contrasting deformation of Sand I-type granitoids in the Lachlan fold belt, eastern Australia. *Tectonophysics* **147**, 127–43.

WAN, B., HEGNER, E., ZHANG, L. C., ROCHOLL, A., CHEN, Z. G., WU, H. Y. & CHEN, F. K. 2009. Re-Os geochronology of chalcopyrite from the Chehugou porphyry Mo–Cu deposit (Northeast China) and geochemical constraints on origin of hosting granites. *Economic Geology* **104**, 351–63.

WHITE, W. H., BOOKSTROM, A. A., KAMILLI, R. J., GANSTER, M. W., SMITH, R. P., RANTA, D. E. & STEININGER, R. C. 1981. Character and origin of Climax-type molybdenum deposits, In *Economic Geology Seventy-Fifth Anniversary Volume, 1905–1980* (ed. B. J. Skinner), pp. 270–316. Economic Geology Publishing Co.

WINDLEY, B. F., KRONER, A., GUO, J., QU, G., LI, Y. & ZHANG, C. 2002. Neoproterozoic to Paleozoic geology of the Altai orogen, NW China: new zircon age data and tectonic evolution. *Journal of Geology* **110**, 719–37.

WU, F. Y., SUN, D. Y. & LIN, Q. 1999. Petrogenesis of the Phanerozoic granites and crustal growth in Northeast China. *Acta Petrologica Sinica* **15**, 181–9 (in Chinese with English abstract).

WU, F. Y., WILDE, S. A., ZHANG, G. L. & SUN, D. Y. 2004. Geochronology and petrogenesis of the post-orogenic Cu-Ni sulfide-bearing mafic–ultramafic complexes in Jilin Province, NE China. *Journal of Asian Earth Sciences* **23**, 781–97.

WU, F. Y., YANG, J. H., WILDE, S. A. & ZHANG, X. O. 2005. Geochronology, petrogenesis and tectonic implications of Jurassic granites in the Liaodong Peninsula, NE China. *Chemical Geology* **221**, 127–56.

WU, H. Y., ZHANG, L. C, CHEN, Z. G. & WAN, B. 2008. Geochemistry, tectonic setting and mineralization potentiality of the ore-bearing monzogranite in the Kulitu molybdenum (copper) deposit of Xar moron metallogenic belt, Inner Mongolia. *Acta Petrologica Sinica* **24**, 867–78 (in Chinese with English abstract).

WU, H. Y., ZHANG, L. C., WAN, B., CHEN, Z. G., XIANG, P., PIRAJNO, F., DU, A. D. & QU, W. J. 2011. Re–Os and $^{40}Ar/^{39}Ar$ ages of the Jiguanshan porphyry Mo deposit, Xilamulun metallogenic belt, NE China, and constraints on mineralization events. *Mineralium Deposita* **46**, 171–85.

WU, F. Y., ZHAO, G. C., SUN, D. Y., WILDE, S. A. & YANG, J. H. 2007. The Hulan Group: its role in the evolution of the Central Asian Orogenic Belt of NE China. *Journal of Asian Earth Sciences* **30**, 542–56.

XIAO, Q. H., DENG, J. F. & MA, D. Q. 2002. *The Ways of Investigation on Granitoids*. Beijing: Geological Publishing House, 294 pp. (in Chinese with English abstract).

XIAO, W. J., WINDLEY, B. F., HAO, J. & ZHAI, M. G. 2003. Accretion leading to collision and the Permian Solonker suture, Inner Mongolia, China: termination of the central Asian orogenic belt. *Tectonics* **22**, 1069, doi:10.1029/2002TC001484.

YANG, J. H., CHUNG, S. L., WILDE, S. A., WU, F. Y., CHU, M. F., LO, C. H. & FAN, H. R. 2005. Petrogenesis of post-orogenic syenites in the Sulu Orogenic Belt, east China: geochronological, geochemical and Nd–Sr isotopic evidence. *Chemical Geology* **214**, 99–125.

YANG, J. H., WU, F. Y., CHUNG, S. L., WILDE, S. A. & CHU, M. F. 2004. Multiple sources for the origin of granites: geochemical and Nd/Sr isotopic evidence from the Gudaoling granite and its mafic enclaves, northeast China. *Geochimica et Cosmochimica Acta* **68**, 4469–83.

ZARTMAN, R. E. & DOE, B. R. 1981. Plumbotectonics: the model. *Tectonophysics* **75**, 135–62.

ZENG, Q. D., LIU, J. M., QIN, F. & ZHANG, Z. L. 2010. Geochronology of the Xiaodonggou porphyry Mo deposit in northern margin of North China Craton. *Resource Geology* **60**, 192–202.

ZENG, Q. D., LIU, J. M., ZHANG, Z. L., CHEN, W. J. & ZHANG, W. Q. 2011*a*. Geology and geochronology of the Xilamulun molybdenum metallogenic belt in eastern Inner Mongolia, China. *International Journal of Earth Sciences* **100**, 1791–1809.

ZENG, Q. D., LIU, J. M., ZHANG, Z. L., QIN, F., CHENG, W. J., YU, C. M. & YE, J. 2009. Ore forming time of the Jiguanshan porphyry molybdenum deposit, north margin of North China Craton and the Indosinian mineralization. *Acta Petrologica Sinica* **25**, 393–8 (in Chinese with English abstract).

ZENG, Q. D., LIU, J. M., ZHANG, Z. L., ZHANG, W. Q., CHU, S. X., ZHANG, S., WANG, Z. C. & DUAN, X. X. 2011*b*. Geology, fluid inclusion, and sulfur isotope studies of the Chehugou porphyry molybdenum–copper deposit, Xilamulun metallogenic belt, NE China. *Resource Geology* **61**, 241–58.

ZHANG, S. H., LIU, S. W., ZHAO, Y., YANG, J. H., SONG, B. & LIU, X. M. 2007. The 1.75–1.68 Ga anorthosite-mangerite-alkali granitoid-rapakivi granite suite from the northern North China Craton: magmatism related to a Paleoproterozoic orogen. *Precambrian Research* **155**, 287–312.

ZHANG, L. C., WU, H. Y., WAN, B. & CHEN, Z. G. 2009. Ages and geodynamic settings of Xilamulun Mo–Cu metallogenic belt in the northern part of the North China Craton. *Gondwana Research* **16**, 243–54.

ZINDLER, A. & HART, S. 1986. Chemical geodynamics. *Annual Review of Earth and Planetary Science* **14**, 493–571.